APPLICATION NOTE

Microstructural and chemical evaluation of a thermally cycled thermal barrier coating system

Introduction

Aerospace engineering is unique among other manufacturing sectors, especially when referring to aerospace engine manufacturing. Engines are the most complex elements in an aircraft, and the need for increased performance has provided the driving force for extensive research around the materials employed.

Engine materials and fabrication technology present several challenges due to the demand of specific mechanical and thermomechanical properties. Engine components must withstand extreme working conditions as they operate at unprecedented levels of temperature, stress and oxidative environments. Consequently, the materials for these kinds of applications need to have temperature and oxidation resistance, high strength, stiffness and fracture toughness. Additionally, factors such as efficiency and cost must be considered. The need for such properties pushed the development of new manufacturing techniques as well as studies around new alloys and surface coatings.

The characterization presented in this application note has been run on a fragment of an afterburner liner of the Pratt & Whitney JT11D engine used in the Lockheed SR-71 aircraft. Specifically, the characterization focuses on the end-of-life, thermally fatigued thermal barrier coating (TBC) used in the afterburner liner.

Figure 1. A jet fighter taking off with full afterburner.

The SR-71 aircraft is a high-speed, high-altitude aircraft, developed and manufactured by the American company Lockheed Corporation in the late 1950s. Some of the 32 SR-71s built during the entire duration of the program were equipped with turbojet engines, which the piece under study comes from. To increase thrust, the JT11D engine used afterburners and additional combustion components that were used on specific types of jet engines as an alternative to bigger engines. Afterburners are generally used only for short durations, where high thrust is required, as they increase the fuel consumption.

An exception to the short duration use is the above-mentioned engine, where the afterburners were used for prolonged periods (more than 15,000 hours of service), showing outstanding thermal fatigue resistance, thanks to the use of TBC on the liner and flame holders.

Figure 2. Rear view of an afterburner.

TBCs are currently employed in various engineering areas. The development of new materials and deposition techniques in the field are key to improve the life of the underlying materials. TBCs have complex structures and must operate in the most demanding high-temperature environment of aircraft and jet engines (the JT11D afterburner had to withstand up to 1700°C). For this reason, the performance of the coating plays a crucial role and continuous efforts are being made to produce improved and durable coatings.

The TBC system under study, as manufactured, has been applied on a Ni-based superalloy afterburner component (Figure 3). The superalloy used as a substrate material is developed as a base material of hot components. Superalloys exhibit excellent mechanical properties against creep and fatigue at high temperatures which allows for extended use in extreme environments. However, they have a limited resistance against high-temperature oxidation and corrosion.

Thus various (Ni,Co)-based metallic coatings are employed to protect the different engine components and to reduce the thermal expansion gradient between the substrate. A first oxidation resistant metallic bond coat has been plasma sprayed over the component (the main reason for using the plasma spray is the large size of the component).

On top of the bond coat, a ceramic top coat is applied. The top layer is in direct contact with hot gasses, hence a material with very low thermal conductivity -such as a ceramic- is employed to decrease the surface temperature of the components.

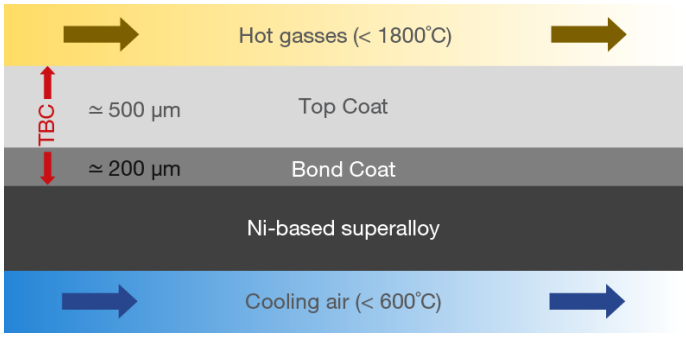

Figure 3. Cross section of the as-manufactured TBC system.

In addition, the coating system contains several arrays of holes over the surface, that act as cooling holes passing through the Ni substrate (Figure 4).

The top coat and the bond coat, combined with the arrays of holes, create a system that has been designed to have a coefficient of thermal expansion (CTE) consistent with the load-carrying capacity of the Ni-based substrate.

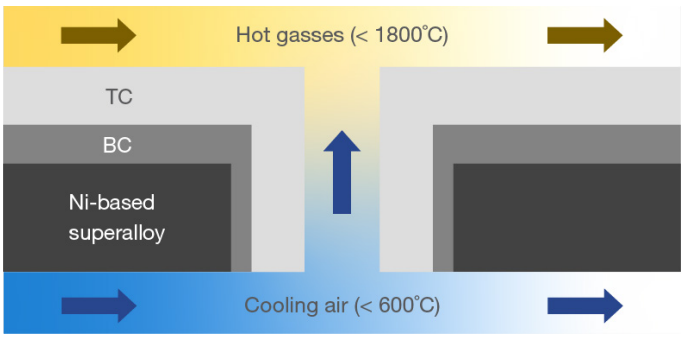

Figure 4. Final as-manufactured system, showing the presence of cooling holes perpendicular to the TBC.

A crucial point to be highlighted in this study is that the analyzed TBC is part of an aircraft that can count 15,000 flight hours; its components underwent huge stresses from several points of view. As all the materials are heavily cycled, it's necessary to treat this specific TBC as an engineering system whose properties have changed with time and cycles during service.

Large area characterization

The sample characterization has been conducted using the new Thermo Scientific™ Axia™ ChemiSEM, a next-generation and alignment-free SEM platform. The Axia ChemiSEM features a new approach for live energy dispersive X-ray (EDS) analysis, with an improved user experience that provides instant, quantitative EDS data even while navigating a sample. The technology is designed to combine the EDS signal with the features in the SEM image, resulting in sharp and accurate EDS images.

A detailed, first overview of the different layers has been obtained using the native image montage creation, which provides an automated acquisition of a large-scale image.

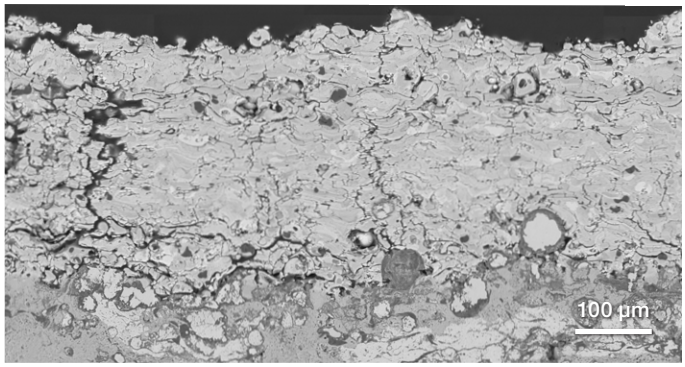

Figure 5. Large scale overview of the TBC layers.

Using only the material contrast provided by the backscattered electron detector (BSE), the wide variety and variability of materials across the layers make it difficult to clarify the compositional variations in the specimen using the BSE image. Thanks to the unique compositional mapping capabilities of the Axia ChemiSEM, the possibility to scan a large portion of the specimen is combined with the quantitative elemental information retrieved from each frame of the montage.

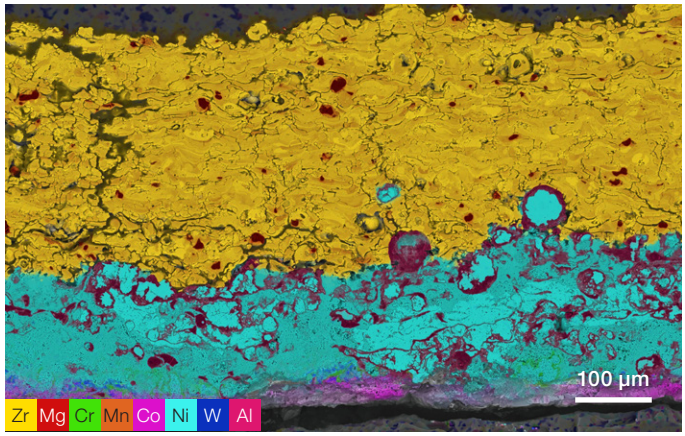

Figure 6. ChemiSEM image of the entire TBC cross section (Acc. voltage 25 keV, beam current 0.64 nA).

The large-scale image in Figure 6 has been acquired by collecting 7x7 tiles and integrating 5 frames for each ROI in order to gain enough X-rays and EDS signal. The whole acquisition took around 30 minutes. In a short time to results, the Axia ChemiSEM provides a clear view of the distribution of the elements to understand the different phases.

Figure 6 identifies at least three different areas of interest. The lower area, displayed in pink, which can be assigned to the superalloy substrate, will be discussed later in more detail.

In addition, it shows a layer in light blue (Ni) that is most likely to be the bond coat. Consistent to the literature, the main alloying elements employed in the bond coat are nickel, cobalt, chromium and aluminum.

The upper layer, in yellow (Zr), can be assigned to the top coat. It also shows the presence of magnesium; magnesium-stabilized zirconia is one of the most employed ceramics for these kinds of applications, thanks to its very low thermal conductivity.

To be noted, the interface between the bond coat and the top coat shows high roughness and inhomogeneities. The arrangement of the layers, while in service, changed compared to the as-manufactured system described above. A thermally grown oxide layer (TGO) certainly developed between the bond coat and the top coat, introducing detrimental residual stresses.

A complete characterization of the different portions is presented in this application note, and the image in Figure 6 has been used as a map to navigate the sample.

Ni-based superalloy substrate

As previously mentioned, the metal substrate is generally made of superalloys. Nickel-based alloys and superalloys are widely used for aerospace, as they provide superior mechanical properties, such as creep and thermal fatigue resistance, at elevated temperatures.

Superalloys usually contain significant amounts of additional alloying elements, up to 10–12, that are added to enhance specific properties such as high-temperature strength, ductility, oxidation resistance and hot-corrosion resistance.

Higher magnification analyses of a portion of the substrate have been conducted using an acceleration voltage of 25 kV and a beam current of 0.33 nA.

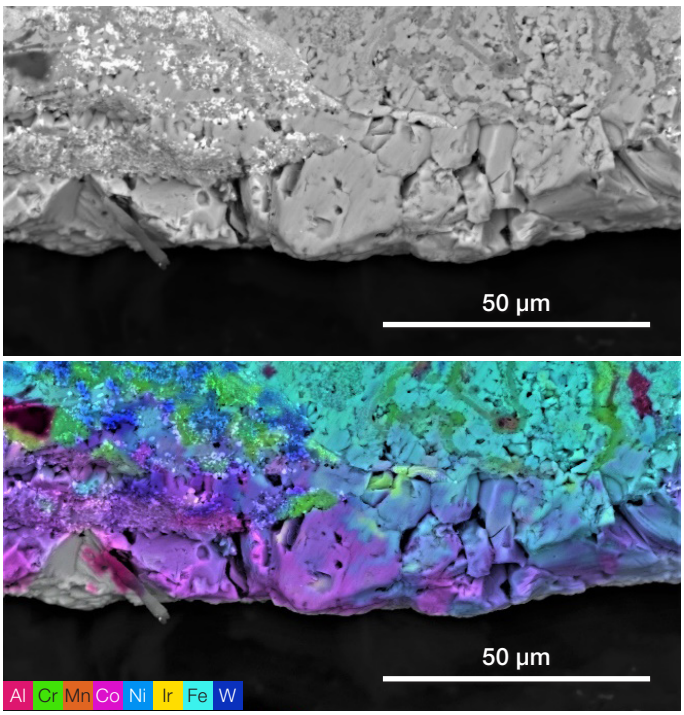

Figure 7. Backscattered electron image of a portion of the metal substrate, on the top, and related ChemiSEM image on the bottom (Acc voltage 25 keV, beam current 0.33 nA).

The set of ChemiSEM images in Figure 7 and Figure 8 were acquired in the same acquisition, which saved time since imaging and elemental analyses are now obtained at the same time. Progressive selection of the different X-ray elemental maps clearly shows an abundance of nickel and cobalt.

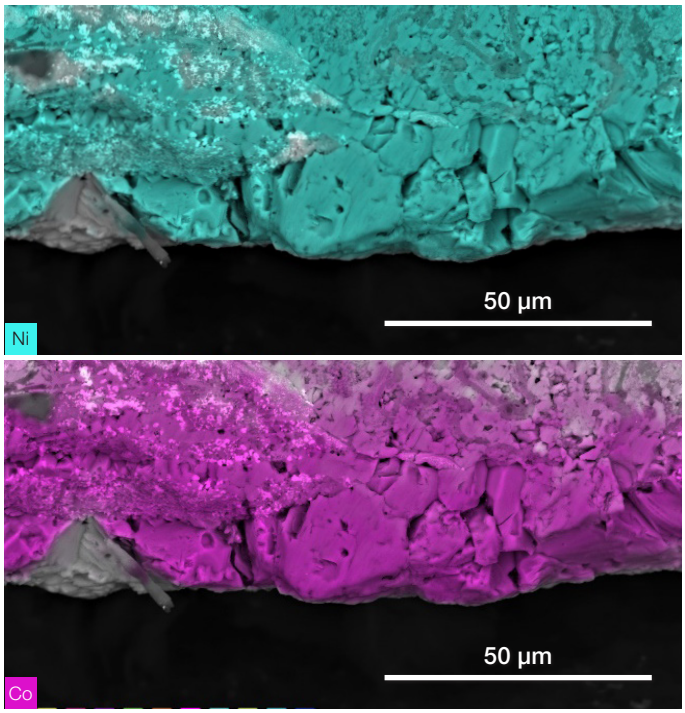

Figure 8. Ni, and Co, ChemiSEM images of the ROI.

Figure 9 shows Cr, Co, and W distribution. Thanks to the possibility to selectively hide or show the elements, the interface between the Ni superalloy and the bond coat is highlighted.

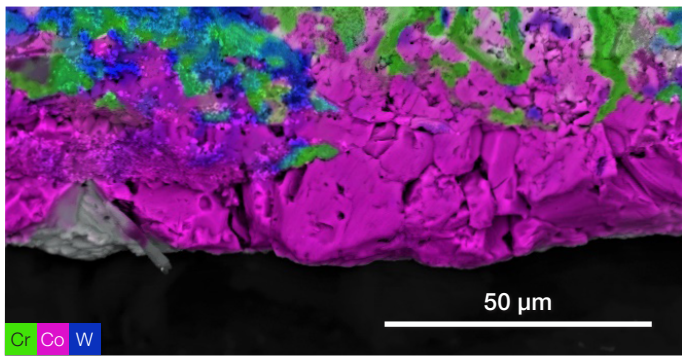

Figure 9. Cr, Co and W ChemiSEM image of the ROI.

Figure 9 shows a clear interdiffusion between the base superalloy and the bond coat, specifically in this case of Cr and W, that have migrated into the bond coat. This is a common thermal fatigue process; phase transformations may happen during the thermal cycles, allowing components from the base metal to diffuse into the upper layer.

MCrAlY alloy bond coat

The bond coat is an oxidation-resistant metallic layer with a variable thickness (200 µm thickness has been measured from Figure 6). It is typically made of a class of alloys referred to as MCrAlY alloys.

MCrAlY alloys (with M = Ni, Co, or both) have been used widely as bond coats in TBCs due to their exceptional oxidation and corrosion resistance at high temperatures. Their main purpose, as an extra metallic layer, is to enhance the oxidation and corrosion resistance of the underlying high-temperature material and to protect it from the environment. These coatings are deposited using electron-beam physical vapor deposition (EB-PV) or plasma spray (APS) methods. In this case, however, plasma spray was used, as previously mentioned, due to the large size of the component on which it was applied.

A detailed characterization of the bond coat layer, both from a microstructural and from an elemental point of view, has been conducted by selecting different regions of interest, as the large-scale overview in Figure 6 showed an inhomogeneous distribution of the materials and elements even within the same layer.

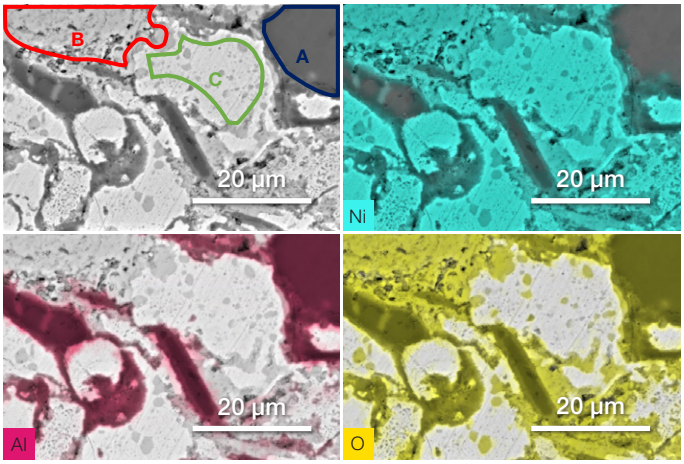

Figure 10. Backscattered electron image (top left) of a close-up of the bond coat. Ni, Al and O ChemiSEM images show the respective elements distribution over the imaged area and highlight the presence of different phases (Acc voltage 25 keV, beam current 0.64 nA).

Figure 10 shows the X-ray images of the most abundant elements in this ROI: Ni, Al and O, respectively. The ChemiSEM oxygen image indicates the presence of oxidation. In TBC systems, oxidation occurs mainly due to the penetration of oxygen through possible existing cracks and porosity in the top coatings (A.A. Vencl, 2019). Such alterations in the top coat may have created the path for corrosive environments, rich in oxygen, nitrogen and sulfur, to penetrate further down to the bond coat and react with it.

Three major phases are recognizable in the ChemiSEM images, as indicated in Figure 10 (top left image), and oxygen is associated to two of them. Point analyses and a linescan have been acquired to disclose their composition and quantify the different elements. The linescan across the three visible phases is presented below.

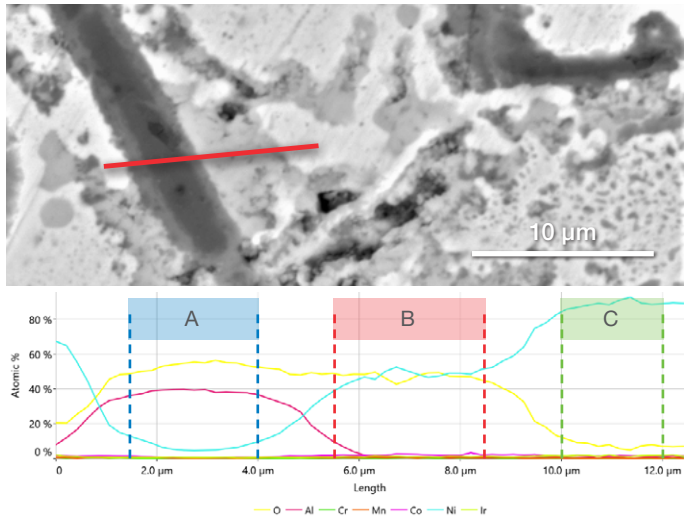

Figure 11. Top image shows the line where the linescan has been acquired. It covers the three different phases highlighted in the previous image (Acc voltage 25 keV, total acquisition time 180 s, average count rate ≈ 10 kcps).

Figure 11 confirms the presence of three different compositions, whose quantifications have been extracted from the linescan data and are reported below, in Figure 12.

	AREA A	AREA B	AREA C
Element	**Atomic %**	**Atomic %**	**Atomic %**
O	56.0	46.1	9.1
Al	42.6	28.5	2.0
Cr	–	0.3	0.8
Mn	–	0.4	0.2
Co	–	1.5	1.4
Ni	0.9	22.7	85.0
Ir	0.5	0.6	1.5

Figure 12. Quantification (Acc voltage 25 keV, beam current 0.64 nA) extracted from the three different ROIs. N.B. the presence of iridium is due to a thin coating which has been sputtered prior to the analysis.

The composition of area A, except for a small amount of nickel, is consistent with the alumina composition. As mentioned above, bond coats during service and thermal cycling tend to form an alumina thermally grown oxide (TGO) layer between the bond coat and the top coat. However, what is clear in the case under study is that aluminum is nonuniformly distributed within the bond coat volume and that the typical TGO is not present.

Doleker et al. (K.M. Doleker, 2018), studied the oxidation behavior and microstructural changes of a magnesia-stabilized zirconia (MSZ) coating employed as a top coat in combination with a CoNiCrAlY metallic bond coat. This specific TBC system was cycled at different temperatures and for a varied number of hours. The study showed that the TGO layer, mostly based on Al_2O_3, exhibited a uniform structure at the initial stages of oxidation. With the increasing oxidation period due to the high amount of service hours, depletion of Al in the coating structure is observed, as we observed in our specimen.

To understand the nature of the other two analyzed areas, consideration needs to be made. MCrAlY coatings are multi-phase materials, and their phase arrangements and ratios may vary depending on the alloy composition.

The microstructure of as-manufactured NiCrAlY and NiCoCrAlY coatings typically consist of two main phases, γ-Ni and β-NiAl, but they may contain other complex phases such as σ-(Cr, Co), γ'-Ni3Al and α-Cr phases in variable amounts depending on the coating composition and temperature (M.M. Morra, 1984) (R. Pillai, 2020).

In this view, area B is consistent with a β-phase, which is generally the richest in Al content. Area C is consistent with a γ-phase, which is a Ni solid solution. This phase may contain minor elements such as Co, Mn, Cr, Al, and the composition of area C in Figure 12, in fact, shows their presence with low atomic percentages. Both β and γ phases in the ROI from Figure 12 appear as oxidized, compared to the as-deposited material. Vencl et al. (A.A. Vencl, 2019), reported the presence of oxide in the bond coat, as already discussed, and it is worth noting that the amount of oxides is described as increasing as the number of thermal cycles increases. The explanation for this behavior has to be found in the top coat. As described in the next section, the thermal cycling of the top coat creates several cracks that develop both horizontally and vertically, generating an interconnected porosity network in the top coat that allows the oxygen to penetrate and diffuse through the bond coat.

Ceramic (magnesia stabilized zirconia) top coat

The ceramic top coat acts as an insulator and is primarily employed to provide protection against high temperature degradation of the materials below, improving the durability of the components. In addition, it lowers fuel consumption. This results in engine performance improvements and in the reduction of the maintenance requirements.

As for the bond coat, the ceramic top coat is commonly deposited using EB-VP or APS. The top coat layer is usually 200–250 µm in thickness and is directly attached to the bond coat.

Zirconia is one of the most employed materials for top coat, thanks to its excellent thermal shock resistance, low thermal conductivity, and a relatively high coefficient of thermal expansion (CTE). However, the zirconia tends to change its crystal structure from tetragonal to monoclinic, thus undergoing possible volumetric changes, which is not advisable when used as a coating (A. Nusair Khan, 2008). For this reason, partially or fully stabilized zirconia is used with various oxides like yttria, ceria, alumina or magnesia added as stabilizers.

In the case under study, zirconia stabilized with magnesia (MSZ) was used, as evident in the quantitative elemental image overview in Figure 5.

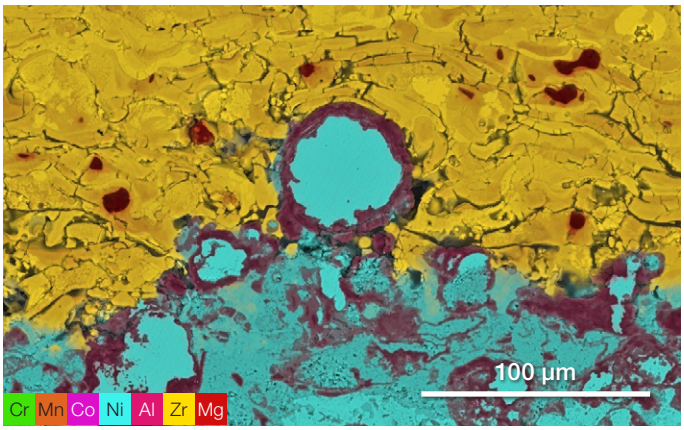

Figure 13. ChemiSEM image of the interface between the bond coat - in light blue - and the top coat - in yellow.

Figure 13 shows the interface between the bond coat and the top coat. Clear information on the microstructure of the top coat becomes evident from the image, especially if compared with the bond coat. The microstructure of MSZ shows, as anticipated in the previous section, the presence of horizontal and vertical cracks, which had not been previously highlighted in the bond coat. These cracks (A.A. Vencl, 2019) are the result of high thermal stresses due to cyclic heating when under service.

High magnification characterization of one portion of this upper layer has been acquired (Figure 14) and confirms the presence of several cracks, mostly horizontal (parallel to the bond coat–top coat interface). The presence of horizontal cracks is one of the main reasons for the failure of TBC systems exposed to thermal cycling, as it causes the delamination of the ceramic top coat.

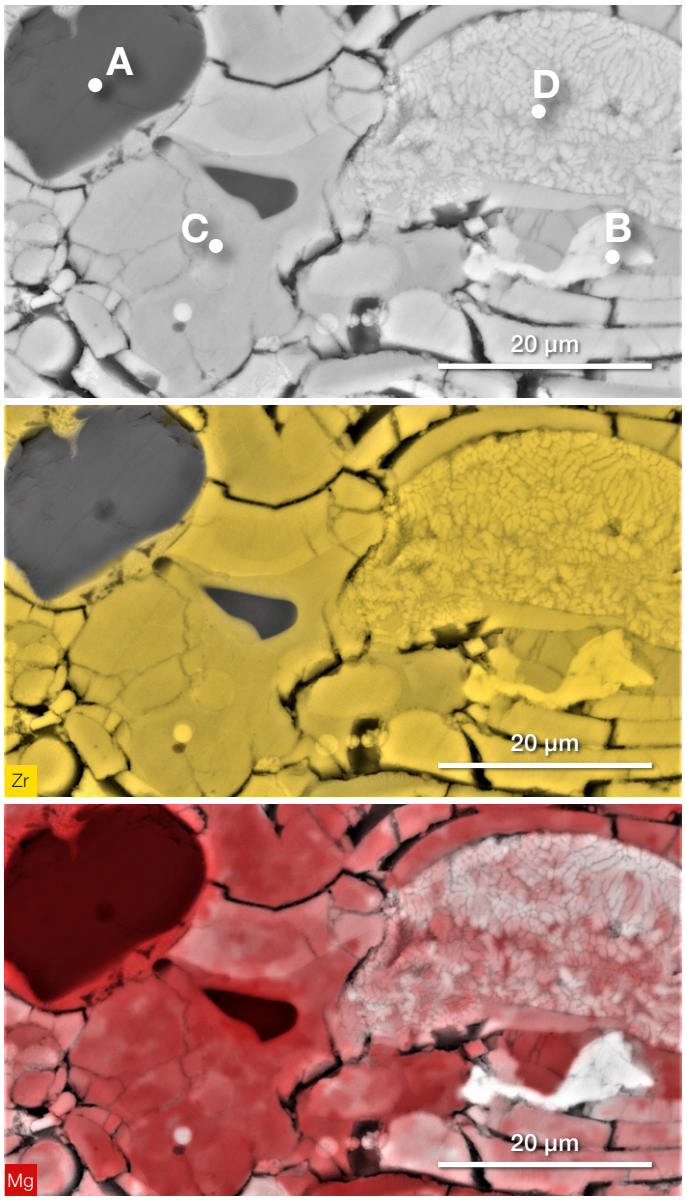

Figure 14. Backscattered electron image (top) and Zr and Mg (middle and bottom) distribution in the top coat (Acc voltage 25 keV, beam current 0.64 nA).

The Zr and Mg ChemiSEM images highlight a different distribution of both elements, suggesting the presence of different phases.

thermoscientific

Element	A at% MgO	B at% ZrO_2	C at%	D at%
O	47	59	42	42
Zr	–	40	30.5	15
Mg	53	–	26.5	42
Ir	1	1	1	1

Figure 15. Point analyses from the different phases of the MSZ top coat (Acc voltage 25 keV, beam current 0.64 nA).

Point analyses run on the points marked in Figure 14 show the presence of pure MgO agglomerates (A) and pure ZrO_2 (B). A possible explanation of the presence of pure MgO is that it was used, together with ZrO_2, as starting material for the plasma spray process, and both raw MgO and ZrO_2 stabilized in situ. However, the most plausible explanation is that an excess of MgO was added in the fully stabilized MSZ.

Regarding the quantitative information extracted from points C and D, it is evident that, aside from the two major phases (zirconia and magnesia) mentioned above, the material underwent intense thermal cycling, which modified the as-manufactured microstructure of the expected material, generating more phases with intermediate compositions as the area C and D, where the ratio between Zr, Mg and O varies with no clear correspondence to either MgO or ZrO_2.

Conclusion

Thermal barrier coatings are very commonly employed in turbine engines, aircraft engines, and for applications where heat insulation of metallic components is required. TBCs are advanced materials systems, and the research around new materials and their combination has become crucial for increased product lifetime. In this view, most studies are focused on the degradation and failure mechanism of the TBCs, with the final goal to obtain layered systems that are capable of resistance, over time and under extreme working conditions, without losing performance.

In this application note, the microstructural and chemical characterization of a TBC is presented. The study revealed heavily evolved microstructures. The system shows the diffusion of various elements and changes in the original structure due to the high temperature creep, leading to the decomposition of the TGO and modification of the bond coat and top coat layers into a mix of various oxides and phases. Voids and cracks, in correspondence with the different layers' alternation, are also visible thanks to the Axia ChemiSEM's capability of large area imaging, with the addition of the elemental information.

With the new Axia ChemiSEM's integrated and always-on EDS system, microstructural information comes together with chemical information for a faster and more efficient method of characterizing the different materials involved.

Reference

A. Nusair Khan I.N. Qureshi Microstructural evaluation of ZrO2–MgO coatings [Journal] // Journal of materials processing technology. - [s.l.] : Elsevier, 2008. - Vol. 209.

A.A. Vencl M.R. Mrdak Thermal cycling behaviour of plasma sprayed NiCr-Al-Co-Y2O3 bond coat in thermal barrier coating system [Journal] // Thermal Science. - 2019. - Vol. 23. - pp. 1789-1800.

K.M. Doleker Y. Ozgurluk, D. Ozkan, N. Mesekiran, A.C. Karaoglanli Comparison of microstructures and oxidation behaviors of Ytria And magnesia stabilized zirconia thermal barrier coatings (TBC) [Journal] // Materials and technology. - June 2018. - Vol. 52. - pp. 315–322.

M.M. Morra R.D. Sisson, R.R. Biederman A microstructural Study of MCrAlY coatings [Book Section] // Surface Engineering. NATO ASI Series (Series E: Applied Sciences) / book auth. Kossowsky R. Singhal S.C.. - [s.l.] : Springer, Dordrecht, 1984. - Vol. 85.

R. Pillai K. Kane M. Lance, B.A. Pint Computational Methods to Accelerate Development of Corrosion Resistant Coatings for Industrial Gas Turbines [Journal] // Superalloys. - [s.l.] : Springer, Cham, 2020. - Vols. The Minerals, Metals & Materials Series. - pp. 824-833.

Find out more at **thermofisher.com/axia-chemisem**

ThermoFisher SCIENTIFIC